INSTITUTE OF PHYSICS PUBLISHING JOURNAL OF PHYSICS B: ATOMIC, MOLECULAR AND OPTICAL PHYSICS

J. Phys. B: At. Mol. Opt. Phys. **35** (2002) 4161–4178 PII: S0953-4075(02)38181-1

Photodetachment of He^- 1s2s2p $^4P^o$ in the region of the 1s threshold

O Zatsarinny[1], T W Gorczyca[1] and C Froese Fischer[2]

[1] Western Michigan University, Kalamazoo, MI 49008, USA
[2] Vanderbilt University, Nashville, TN 37235, USA

Received 14 June 2002, in final form 19 July 2002
Published 1 October 2002
Online at stacks.iop.org/JPhysB/35/4161

Abstract

Photodetachment cross sections of the He^- 1s2s2p $^4P^o$ metastable state in the region of the 1s threshold (38–52 eV) have been calculated using a modified R-matrix method based on a B-spline representation of the scattering orbitals. An accurate representation of initial state and target state wavefunctions has been obtained using a basis of non-orthogonal orbitals. The 17 bound (1s2l, 1s3l) and autoionizing (2l2l', 2l3l') states of He have been included in the close-coupling (CC) expansion. The convergence of the CC expansion has been checked by inclusion of additional 1s4l, 1s5l and 3l3l' target states. Close agreement was found with recent high-resolution K-shell photodetachment measurements of He^- giving rise to He^+ ions (Berrah N, Bozek J D, Turri G, Akerman G, Rude B, Zhou H L and Manson S T 2002 *Phys. Rev. Lett.* **88** 93001), except for the threshold maximum above the first 1s detachment threshold 2s2p $^3P^o$ at 38.88 eV, where the theoretical cross section is a factor of two larger than experiment. Our results show 1s photodetachment cross sections with numerous structures which have been analysed in detail. A set of triply excited resonances is also found, and their energy positions, widths and decay branching ratios are presented.

1. Introduction

The structure of a negative ion is intrinsically different from that of an atom or a positive ion due to the more extensive screening of the nucleus by the electrons. This causes the inter-electronic interactions to become relatively more important, and the enhanced correlation can dominate the structure and dynamics of these weakly bound systems. The photodetachment process of negative ions stands out as an extremely sensitive probe of negative-ion properties and provides a sensitive test of the ability of theory to go beyond the independent-electron model. Up to recent times, most of the theoretical results and experimental data were related to photodetachment processes in which only one or two outer subshells are involved (see, for example, Buckman and Clark 1994, Ivanov 1999), whereas inner-shell photodetachment has been largely unexplored.

The situation changed over the last few years when several calculations (Amusia *et al* 1990, Ivanov *et al* 1998, Xi and Froese Fischer 1999, Zhou *et al* 2001a) predicted strong many-body effects in the photodetachment of deep inner shells. This encouraged experimentalists to extend measurements to higher energies. Besides, the advent of third-generation synchrotron light sources, with higher flux, brightness and resolution, made it possible to investigate experimentally inner-shell processes in tenuous negative ion targets. As a result, measurements of inner-shell photodetachment have been made for several elements: Li^- (Kjeldsen *et al* 2001, Berrah *et al* 2001), Na^- (Covington *et al* 2001) and He^- (Berrah *et al* 2002). The measurements displayed dramatic structures differing substantially from the corresponding processes in neutral atoms and positive ions.

This difference might not be expected at first since deep inner shells of negative ions are essentially unaffected by the very diffuse cloud of outer-shell electrons, and the static properties of these deep inner-shell electrons are very close to those of the corresponding positive ions. However, this is not necessarily true for dynamic properties, especially electron detachment, where an inner-shell electron exiting the system must pass through the diffuse cloud of outer-shell electrons, resulting in additional resonance structure. As a whole, there is a good qualitative agreement between experiment and R-matrix calculations for the 1s photodetachment in He^- and Li^- (Berrah *et al* 2001, Zhou *et al* 2001b), but the calculated cross section in the first 1s threshold exceeds measurement by more than a factor of two for both He^- and Li^-. The narrow resonance structure in the higher-energy region was not analysed in detail.

In this paper, we present new R-matrix calculations for photodetachment of the $1s2s2p\,^4P^o$ state of He^- in the high-energy region, in order to resolve the existing discrepancies between experiment and theory, as well as considerable discrepancies between different calculations. The first theoretical study of photodetachment of He^- in the 1s threshold region was undertaken using the multiconfiguration Hartree–Fock (MCHF) wavefunctions for discrete states and a continuum configuration-interaction (CI) method for resonances (Kim *et al* 1997). Coupling between open channels was not, however, included. A more rigorous and detailed investigation of photodetachment of He^- was performed by Xi and Froese Fischer (1996, 1999) using a new method based on direct solution of the close-coupling (CC) equations using a B-spline basis. More recently, the photodetachment cross section of He^- in the region of the 1s threshold has been calculated by Zhou *et al* (2001a) using a standard R-matrix code with an enhanced asymptotic treatment, modified to handle a negative-ion system. The results show a 1s photodetachment cross section with numerous structures which were ascribed to the dominance of correlation of both initial and final states of negative ions. Comparison with previous calculations shows that while there are some areas of excellent agreement, overall there are serious discrepancies. To resolve these discrepancies and discrepancies between theory and experiment is the main motivation of the present work. Note also that very recent calculations of Sanz-Vicario and Lindroth (2002), based on the complex rotation CI method, confirm the main features of the R-matrix calculations of Zhou *et al* (2001a).

In order to calculate photodetachment cross sections, we used the new R-matrix program (Zatsarinny and Froese Fischer 2000, Zatsarinny and Tayal 2001a, 2001b), which has some new features compared to standard R-matrix treatment. First, emphasis is placed on the accuracy of target wavefunctions by using non-orthogonal orbitals; these are optimized for each atomic state separately. For the description of continuum orbitals, we use a B-spline basis, and do not impose any orthogonality constraints between continuum and spectroscopic, or correlated, atomic orbitals. Thus, in principle, we do not need any $(N + 1)$-electron terms in the CC expansion to compensate for the artificial orthogonality constraints on the continuum orbitals, which are imposed in the standard R-matrix treatment. That simplifies the calculations and leads to a substantial reduction in the pseudo-resonance structure at higher energies.

In this paper, we present partial and total cross sections for the photodetachment of the He^- 1s2s2p $^4P^o$ metastable state in the 1s threshold region (photon energy region from 38.8 to 52 eV). The calculations have been done in the LS coupling scheme in two approximations, with the R-matrix CC expansion consisting of 17 and 31 target states. This allows us to explore the convergence of the CC expansion. We also intend to provide a more complete study of the resonance structure.

2. Computational details

2.1. Target wavefunctions

The accurate representation of the target wavefunctions is an important component of any reliable scattering calculation. The He-like wavefunctions are well studied in the literature and, in principle, can be obtained with extremely high accuracy. However, in the scattering calculations, when the same orbital set is used to generate all target wavefunctions as well as the initial state wavefunction, the accurate generation even of relatively simple He-like wavefunctions may need extremely large CI expansions. In this case, special optimization algorithms should be used to produce the best average result with a reasonable number of configuration state functions. For example, Xi and Froese Fischer (1999) generated orbitals with $n \leqslant 5$ from consideration of the 1snl bound states. Additional correlation orbitals were optimized so that the best average results could be obtained for the initial state, and target autoionizing states, of interest. Specifically, orbitals with $n = 6, 7, 8$ were optimized for the 2s2p ^3P state, and orbitals with $n = 9, 10$ were optimized for the initial state. This procedure leads to accurate target states but with extremely large configuration expansions. A similar procedure was also used by Zhou *et al* (2001a) but with a much more limited set of correlated orbitals to ensure that the R-matrix calculation did not become too large.

In order to obtain an adequate representation of the target states in the present work, we used an alternative method for generating radial orbitals, based on a detailed examination of the different correlation effects, and inclusion of the main correlation with specific configurations, or with specific correlated orbitals. This approach has no simple systematic procedure, but can lead to rather accurate results with a relatively small number of configurations. In this respect, use of the non-orthogonal orbitals can provide a more flexible procedure. The general formalism does not require orthogonality of one-electron radial functions but only the orthogonality of total atomic wavefunctions. As we will see below, use of non-orthogonal orbitals allows us to include correlation with a minimum number of configurations and correlated orbitals. This approach has been successfully applied to the generation of target states in lithium (Zatsarinny and Froese Fischer 2000), oxygen (Zatsarinny and Tayal 2001a) and sulfur (Zatsarinny and Tayal 2001b), where it was very effective for the description of open-shell atoms. In general, the non-orthogonal technique, compared to the orthogonal orbital technique, leads to a much more time-consuming calculation of matrix elements but provides much larger flexibility in the choice of target wavefunctions which now can be obtained from independent calculations.

The bound 1s2l and 1s3l target states of He have been obtained from a set of separate independent MCHF calculations, similar to the case of Li^+ target states used by Zatsarinny and Froese Fischer (2000). This leads to non-orthogonal one-electron orbitals for different states but gives the minimum number of configuration state functions required to achieve the same level of accuracy for target wavefunctions as in Xi and Froese Fischer (1999). The $n = 4, 5$ bound orbitals were obtained from the HF $1snl\ ^3L$ calculations with a hydrogenic 1s orbital. The next step was to obtain wavefunctions for autoionizing target states. This was done in the independent calculations as follows. We start from configuration expansions based on hydrogenic $n = 2$–5 orbitals as the initial approximation. Then for each term we generated the 6s–6g correlated orbitals optimized on the corresponding lowest autoionizing state. Examples are the 2s2p state for the $^3P^o$ term or $2p^2$ for the ^3P term. If the results for some states were not converged, we additionally generated the 7s–7g correlated orbitals optimized on this specific state. For example, we used additional orbitals for the 2p3p ^3P state. Finally, the target wavefunctions for a given term were obtained from CI calculations where a final configuration expansion was combined with corresponding configuration expansions for bound and autoionizing states. This guarantees the orthogonality of target wavefunctions. All final configuration expansions were restricted to configurations with weights $c > 0.0001$.

Resulting energies of the target states are compared in table 1 with energies obtained in the calculations of Xi and Froese Fischer (1999) and Zhou *et al* (2001a), as well as with the most accurate energies which we could find in the literature for these states. The achieved accuracy is of the order of 10^{-5} au for bound states, and of the order of 10^{-3} au for the autoionizing states. Comparing the energies of autoionizing states, we should take into account the fact that the accurate results of Lindroth (1994) and Ho (1993) also contain the shift due to interaction with the continuum, which can achieve the value of 10^{-3} au. The achieved accuracy of total energies is comparable to the accuracy obtained by Xi and Froese Fischer (1999). However, we used a far smaller configuration expansion which consisted of 30–70 configuration state functions, depending on the term under consideration. The reduction of the configuration expansion has been obtained at the price of a large number of different one-electron orbitals (98 different orbitals were used for representing all target states in the present calculations). On the other hand, the computational time depends mainly on the size of the configuration expansion, and the large number of one-electron functions does not complicate the calculations.

Comparison of oscillator strengths for transitions between target states can provide an additional test of the reliability of the present wavefunctions. For transitions between bound states we obtained very close agreement (within 1%) between length and velocity forms, and with the results of Chen (1994). The calculations of Chen (1994) were carried out with extensive B-spline expansions and should be considered the most accurate to date. We also obtained good agreement with the results of Zhou *et al* (2001a) for transitions to autoionizing states. Note, however, that for some transitions with small f-values (<0.01) the length and velocity forms agree closely in both calculations, but the oscillator strengths differ considerably, especially in the case of transitions to the 2s2p, 2s3p, 2p3s $^3P^o$ autoionizing states. On the basis of the above comparison of target energies and oscillator strengths, we can conclude that our wavefunctions include the dominant correlation and provide a good representation of the target states in the R-matrix calculations.

The initial 1s2s2p $^4P^o$ state was obtained in the independent MCHF calculations, using a straightforward active-set approach, and generating all possible configuration state functions from active set orbitals with $n = 1$–5. As can be seen in table 1, the resulting total energy is close to the accurate results of Kristensen *et al* (1997). It should be noted that the 2s and 2p orbitals here differ considerably from the corresponding orbitals in the target states. This indicates large relaxation effects during the 1s photodetachment, which are directly included in the present calculations. The small residual difference in excitation energies, which affects the position of resonances, can be removed by using the exact or experimental energies for the initial and target states.

Table 1. Energy (in au) of target states and their relative value (in eV) to the 1s2s2p ^{4}P initial state (1 au = 27.207 652 eV is used to convert au to eV).

Target	Present	Xi and Froese Fischer (1999)	Zhou *et al* (2001)	Others	Relative value (eV)
1s2s2p ^{4}P	−2.178 015	−2.178 050	−2.177 933	−2.178 073[a]	0.0
1s2s ^{3}S	−2.175 225	−2.175 202	−2.175 117	−2.175 229[b]	0.076
1s2p ^{3}P^o	−2.133 139	−2.133 157	−2.132 969	−2.133 164	1.221
1s3s ^{3}S	−2.068 684	−2.068 683	−2.068 656	−2.068 689	2.974
1s3p ^{3}P^o	−2.058 071	−2.058 058	−2.058 019	−2.058 081	3.263
1s3d ^{3}D	−2.055 634	−2.055 636	−2.055 604	−2.055 636	3.330
2s2p ^{3}P^o	−0.760 860	−0.760 458	−0.758 251	−0.760 492[c]	38.564
2p^2 ^{3}P	−0.710 465	−0.710 492	−0.708 737	−0.710 500[d]	39.930
2s3s ^{3}S	−0.602 578	−0.602 486	−0.600 375	−0.602 578[d]	42.864
2s3p ^{3}P^o	−0.584 724	−0.584 580	−0.582 778	−0.584 672[c]	43.349
2p3p ^{3}D	−0.583 781	−0.583 669	−0.580 561	−0.583 784[c]	43.377
2p3s ^{3}P^o	−0.578 889	−0.578 990	−0.576 099	−0.579 031[c]	43.512
2p3p ^{3}P	−0.567 799	−0.567 729	−0.565 061	−0.567 81[d]	43.810
2p3d ^{3}F^o	−0.565 141	−0.565 928	−0.560 656	−0.566 20[d]	43.879
2s3d ^{3}D	−0.560 630	−0.560 198	−0.556 172	−0.560 687[c]	44.006
2p3p ^{3}S	−0.559 720	−0.558 841	−0.557 148	−0.559 747[d]	44.035
2p3d ^{3}D^o	−0.559 312			−0.559 30[d]	44.044
2p3d ^{3}P^o	−0.548 681	−0.548 813	−0.545 521	−0.548 844[c]	44.329
1s4s ^{3}S	−2.036 510			−2.036 512[b]	3.852
1s4p ^{3}P^o	−2.032 313			−2.032 324	3.965
1s4d ^{3}D	−2.031 287			−2.031 289	3.994
1s5s ^{3}S	−2.022 617			−2.022 619	4.230
1s5p ^{3}P^o	−2.020 544			−2.020 551	4.286
1s5d ^{3}D	−2.020 020			−2.020 021	4.300
3s3p ^{3}P^o	−0.351 137			−0.350 378[d]	49.727
3p^2 ^{3}P	−0.338 106			−0.336 088	50.116
3p3d ^{3}F^o	−0.331 526			−0.331 64	50.237
3s3d ^{3}D	−0.326 491			−0.325 331	50.409
3p3d ^{3}D^o	−0.316 186			−0.315 575	50.674
3d^2 ^{3}F	−0.310 467			−0.310 725	50.806
3p3d ^{3}P^o	−0.308 994			−0.309 380	50.843
3d^2 ^{3}P	−0.290 460			−0.291 158	51.338

[a] Kristensen *et al* (1997), Bylicki and Pestka (1996).
[b] Kono and Hattori (1984).
[c] Ho (1993).
[d] Lindroth (1994).

2.2. Photodetachment calculations

Photodetachment calculations have been carried out using the new R-matrix code, in which non-orthogonal orbitals are used for describing both the target states and the R-matrix continuum basis functions. In particular, a B-spline basis is used for the description of continuum functions in the internal region. The details of the method have been given by Zatsarinny and Froese Fischer (2000) and by Zatsarinny and Tayal (2001a, 2001b). Here, we give a brief outline.

As in the standard R-matrix method (Burke and Berrington 1993), the wavefunction describing the total $(N+1)$-electron system in the internal region with $0 < r < a$ is expanded in terms of energy-independent functions

$$\Psi_k = A \sum_{ij} a_{ijk} \bar{\Phi}_i u_j(r) + \sum_j b_{jk} \phi_j \tag{1}$$

where $\bar{\Phi}_i$ are channel functions formed from the N-electron target states Φ_i (physical and pseudo) included in the close coupling expansion, u_j are the radial basis functions describing the motion of the scattering electron, and ϕ_j are $(N+1)$-electron bound configurations which allow for short-range correlation effect and completeness. In our implementation of the R-matrix method, the radial functions u_j are expanded in the spline basis as

$$u_j(r) = \sum_i \bar{a}_{ij} B_i(r), \tag{2}$$

where the coefficients $\bar{a}_{ij}$ (which now replace the coefficients a_{ijk} in equation (1)) and coefficients b_{jk} are found by diagonalizing the $(N+1)$-electron Hamiltonian inside the R-matrix box of radius a. Use of the B-spline basis leads to a generalized eigenvalue problem of the form

$$\boldsymbol{Hc} = E\boldsymbol{Sc}, \tag{3}$$

where $\boldsymbol{S}$ is the overlap matrix, which in the case of the usual orthogonal conditions on scattering orbitals reduces to the banded matrix, consisting of overlaps between individual B-splines, but in the more general case of non-orthogonal orbitals has more complicated structure (Zatsarinny and Froese Fischer 2000). For an accurate determination of the electron flux through the boundary, we do not impose any boundary conditions on the u_j functions at the outer edge of the box. In order to obtain the Hermitian interaction matrix in the internal region, we add the Bloch operator to the Hamiltonian (Burke and Berrington 1993). The amplitudes of the wavefunctions at the boundary which are needed for construction of the R-matrix are simply given by the coefficient of the last spline, the only spline which has nonzero value at the boundary.

The choice of B-splines as basis functions has certain advantages. The B-splines are bell-shaped piecewise polynomial functions of order k_s (degree $k_s - 1$) and defined by a given set of points in some finite radial interval. They were introduced into atomic structure calculations about ten years ago and have been widely used due to their excellent numerical approximation properties (for reference, see the recent review by Bachau *et al* (2001)). The important property of B-splines is that they form an effectively *complete* basis on the interval spanned by the knot sequence. The completeness of the B-spline basis ensures that no Buttle correction to the R-matrix elements is required.

R-matrix calculations were carried out with the following parameters. The R-matrix radius $a = 100$ au is chosen to ensure that the bound orbitals approach zero at the boundary. The number of continuum basis functions $u_j(r)$ for each orbital angular momentum was 150. This number of continuum basis functions is considerably larger than in standard R-matrix calculations. In the present approach, this number is defined by the number of B-splines, which in turn is defined by the choice of grid. It is necessary to use the grid with maximum step value of $1/k$, where k is the maximum linear momentum of the incident electron; otherwise, the B-spline basis inadequately describes the oscillating behaviour of the wavefunction. Scattering parameters are then found by matching the inner solution at $r = a$ to asymptotic solutions in the outer region. The ASYPCK program (Crees 1980) has been employed to find the asymptotic solutions. In the present scattering calculations, we do not impose any orthogonality conditions on the scattering orbitals, and that allows us to avoid the introduction of the additional $(N+1)$-electron terms in the CC expansion which are usually used to compensate the orthogonality constraints on the scattering orbitals.

Since the initial state is He^- 1s2s2p $^4P^o$, the final continuum states, by dipole selection rules, must be ^4S, ^4P, or ^4D. The calculations of dipole matrices between the initial state and final continuum functions have been done on the basis of non-orthogonal orbitals with full inclusion of relaxation effects (Zatsarinny 1996). In the first step, the CC expansion included 17 target states (the 1s2l and 1s3l bound states and all $2l2l'$ and $2l3l'$ autoionizing states of He—approximation 17CC). This is almost the same CC expansion as in previous calculations by Xi and Froese Fischer (1999) and Zhou *et al* (2001a), except that we excluded the 2s4s ^3S state and included the 2p3d $^3D^o$ state. We regard the inclusion of all $2l3l'$ states as more consistent. In the second step, in order to explore the convergence of the CC expansion, we additionally included the 1s4l, 1s5l and $3l3l'$ target states—approximation 31CC. The number of target states in this case is equal to 31, with the number of different scattering channels equal to 24, 32 and 60 for $^4S^e$, $^4P^e$ or $^4D^e$ partial waves, respectively.

2.3. Resonance analysis

For detection and parametrization of resonances we use the time-delay matrix method. This method for analysis of resonances has been proposed by Smith (1960), and is based on the introduction of a time-delay matrix $\boldsymbol{Q}$, which is formed from the scattering matrix $\boldsymbol{S}$ and the time operator $-\mathrm{i}\,\mathrm{d}/\mathrm{d}E$:

$$\boldsymbol{Q} = -\mathrm{i}\boldsymbol{S}^* \frac{\mathrm{d}\boldsymbol{S}}{\mathrm{d}E}. \tag{4}$$

Smith showed that the largest eigenvalue of the $\boldsymbol{Q}$-matrix, q, represents the longest time-delay of the incident particle. He further showed that the probability of decay into a particular channel, the branching ratio, is given by the square of the corresponding component of the eigenvector associated with q. Close to resonance, the time-delay has a Lorentzian form given by

$$q(E) = \frac{\Gamma}{(E - E_0)^2 + (\Gamma/2)^2}, \tag{5}$$

where E is the incoming projectile energy, E_0 is the position and Γ is the width of the resonance. At resonance ($E - E_0$), the time-decay function has a maximum with, in atomic units, height $= 4/\text{width}$.

The computation can be split into two parts. The first part calculates the time-delay as a function of energy, and the second locates and fits resonances using equation (5). For determination of the $\boldsymbol{Q}$ matrix, we used the energy derivative of $\boldsymbol{S}$ found numerically with energy step 10^{-6} Ryd.

The resonance analysis based on the time-delay matrix method is seldom used in the photoionization or electron-scattering calculations. This method requires additional calculation of the scattering matrix, which can considerably increase the computational time compared to direct fitting of photoionization cross sections according to known resonant cross section dependences. On the other hand, the time-delay matrix method directly provides the partial and total width, even in the case of complicated structure due to overlapping resonances, where the fitting of cross sections is problematic. The same concerns resonances located close to excitation thresholds. The ^4S partial photodetachment cross section, discussed in the next section, is one particular example in this respect.

3. Results and discussion

Photodetachment of the 1s2s2p $^4P^o$ metastable states, due to LS selection rules, leads to the three final states with ^4S, ^4P and ^4D terms. We first discuss the partial cross sections to the ^4S, ^4P

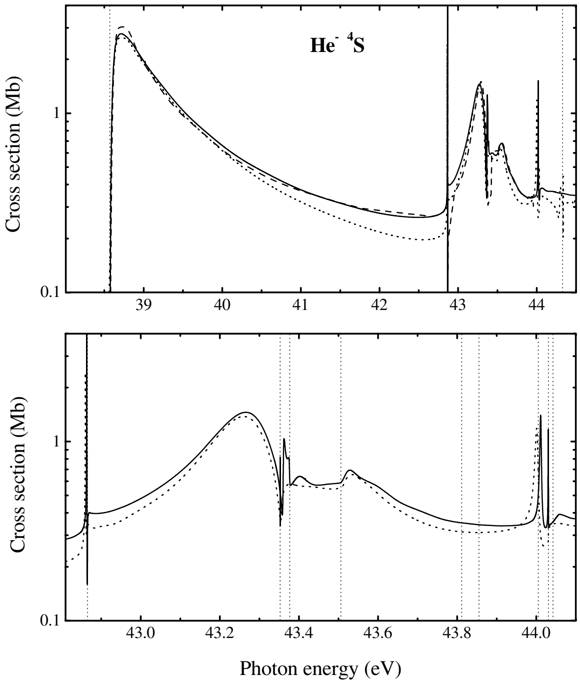

Figure 1. Calculated photodetachment cross sections to the He$^-$ ^{4}S final states. Solid curve, present R-matrix results in the 17CC approximation; dashed curve, R-matrix calculations of Zhou *et al* (2001a); dotted curve, complex scaled CI results of Sanz-Vicario and Lindroth (2002). The vertical lines indicate the He excitation thresholds.

and ^{4}D final states separately for more detailed comparison with other calculations. The partial cross sections obtained in the 17-target-state approximation are presented in figures 1–3 for the ^{4}S, ^{4}P and ^{4}D terms, respectively. The comparison is given with the recent R-matrix calculations of Zhou *et al* (2001a), and with complex-rotation calculations of Sanz-Vicario and Lindroth (2002). We do not compare with a spline–Galerkin calculation of Xi and Froese Fischer (1999). The detailed comparison has been carried out in the above-mentioned works and it has been shown that, although the ^{4}S and ^{4}P partial cross sections of Xi and Froese Fischer (1999) agreed with recent calculations, the dominant ^{4}D partial cross section somehow seemed incorrect. The photon energy in our calculations ranges from 38 to 44 eV. In the photon energy region of the 1s photodetachment, the final target states include the doubly excited states of neutral helium with $n, n' > 1$. Direct photodetachment of the 1s electron leads only to the 2s2p ^{3}P^o target state, whereas other target states can be reached through the 1s photodetachment plus target excitation. So, we can expect the largest cross section at the 2s2p ^{3}P^o threshold. Besides, the 2s and 2p orbitals in the initial 1s2s2p ^{4}P^o state are much more diffuse than in the doubly excited states of neutral helium. This can lead to large shake-up probabilities for population of other ^{3}P^o states (2s3p, 2p3s, 2p3d, 3s3p). During 1s excitation, He$^-$ can also reach triply excited states. The autoionization of these states leads to strong resonance structure in the photodetachment cross sections.

3.1. ^{4}*S photodetachment cross section*

The cross section to the final ^{4}S state is shown in figure 1. In order to simplify the figures, we present hereafter only the cross sections in the velocity form. The cross sections in the

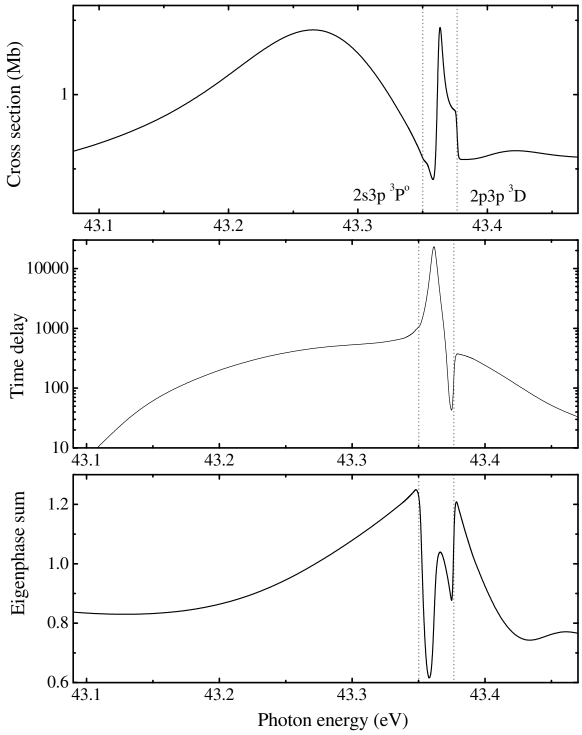

Figure 2. Photodetachment cross section, time-delay function and eigenphase sum for the ^{4}S partial wave in the region of the ^{4}S(2) resonance.

velocity and length forms agree closely with each other, and the difference does not exceed 1% for all energies. We see rather good agreement between the different calculations, except for the narrow resonance structure at higher energies. The first peak of the ^{4}S cross section at 38.7 eV is the result of photodetachment to the (2s2p ^{3}P)kp channel. As mentioned by Zhou *et al* (2001a), this peak is not a resonance but threshold behaviour.

A complicated resonance structure is detected in the energy region 43–44 eV, close to the position of the $2l3l'$ target states. All calculations show a narrow Feshbach resonance 2s3s4s located just below the He 2s3s ^{3}S threshold, but the position, and especially the width, differs considerably in the different calculations. The comparison of positions and widths for some well established resonances is given in table 2. Accurate values for the He excitation thresholds are crucial for locating resonance positions, and the difference in the resonance positions is mainly caused by differences in the target state energies. On the other hand, the large difference in width for the lowest 2s3s4s resonance indicates the importance of correlation corrections. Our calculations, and the R-matrix calculations by Zhou *et al* (2001a), include approximately the same level of multichannel interaction, and differ mainly in the accuracy of the doubly excited target state description. Accuracy of target state description obviously influences all calculated parameters of quasibound states in He$^-$.

The broad feature located around 43.3 eV is a matter of controversy. Zhou *et al* (2001a) claim that this is not due to a resonance, but rather that the complicated behaviour of the ^{4}S cross section around 43.3 eV is most probably due to interchannel coupling effects, coupled with the fact that photodetachment cross sections rise from zero at threshold; this only gives the appearance of resonances. According to the complex scaling calculations of Sanz-Vicario and

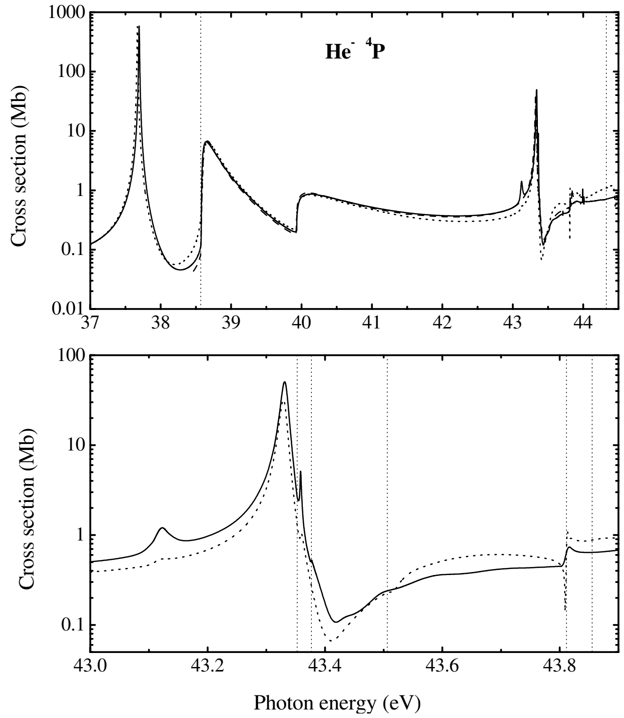

Figure 3. Calculated photodetachment cross sections to the He^- ^4P final states. The notation is the same as in figure 1.

Lindroth (2002), this peak is associated with a pole of the *S*-matrix, and the authors conclude that it is a broad resonance. Our identification of resonances is based on the time-delay method and the analysis of the eigenphase sum. These functions, along with the cross sections, are presented in figure 2. We see that the eigenphase sum does not change by π in this region (as well as in the region of the following narrow peaks at 43.37 eV), and the time-delay function in this region does not exhibit a simple Lorentzian shape, as we have found in the case of other resonances. Nevertheless, the total change of eigenphase in the region of the broad and narrow maxima is close to π. The time-delay functions also can be considered as a broad Lorentzian shape, perturbed by two excitation thresholds, 2s3p $^3P^o$ and 2p3p ^3D. It is interesting to note that the narrow maximum at 43.37 eV also exhibits a Lorentzian form, but with much smaller width. We fitted both these maxima, and the corresponding data are presented in table 3 as resonances $^4S(2)$ and $^4S(3)$. Our interpretation of this resonance structure, however, is not as due to the overlap of two resonances, but as one broad resonance perturbed by the 2s3p $^3P^o$ and 2p3p ^3D excitation thresholds. This causes an unusual resonance structure, with two peaks in the photodetachment cross section, which cannot be fitted accurately to analytical forms widely used in the analysis of resonance structure. An additional complication is due to the cusp near the 2p3p ^3D threshold. The above example shows the advantage of the time-delay matrix method for the analysis of complicated structures. Note also that our width of the $^4S(2)$ resonance in table 3 is close to the value of 208 meV predicted by Brandefelt and Lindroth (2002).

The next prominent feature in the ^4S cross section is observed at 44.017 eV. We identify this as the 2p3d4p resonance. As seen from table 2, our position of this resonance agrees closely with the results of the complex rotation calculations of Brandefelt and Lindroth (2002). However, the width of this resonance differs by a factor of two. This resonance is located toward the

Table 2. Positions and widths of the He^- resonances compared with those from other theoretical calculations.

State	Position (eV)	Width (meV)	Method	Reference
$2s2p^2\ ^4P$	37.672	10.3	Complex-coordinate rotation	Bylicki and Nicolaides (1995)
	37.670	9.87	Saddle-point complex rotation	Chung (1995)
	37.669	9.85	*B*-spline CC, 17CC	Xi and Froese Fischer (1999)
	37.703	9.74	*R*-matrix, 17CC	Zhou *et al* (2001a)
	37.669	9.66	*B*-spline complex rotation	Sanz-Vicario and Lindroth (2002)
	37.692	10.2	*B*-spline *R*-matrix, 17CC	Present
	37.685	10.8	*B*-spline *R*-matrix, 31CC	Present
$2p3s3p\ ^4P$	43.353	12.6	*B*-spline CC, 17CC	Xi and Froese Fischer (1999)
	43.370	14.4	*R*-matrix, 17CC	Zhou *et al* (2001a)
	43.330	13.8	*B*-spline complex rotation	Sanz-Vicario and Lindroth (2002)
	43.336	13.6	*B*-spline *R*-matrix, 17CC	Present
	43.332	14.0	*B*-spline *R*-matrix, 31CC	Present
$3s3p^2\ ^4P$	48.994	154	Saddle-point complex rotation	Chung (2001)
	48.997	141	*B*-spline *R*-matrix, 31CC	Present
$2s3s4s\ ^4S$	42.866	0.103	*B*-spline CC, 17CC	Xi and Froese Fischer (1999)
	42.919	0.120	*R*-matrix, 17CC	Zhou *et al* (2001a)
	42.864	0.350	*B*-spline complex rotation	Brandefelt and Lindroth (2002)
	42.860	0.544	Complex scaled CI	Sanz-Vicario and Lindroth (2002)
	42.862	0.168	*B*-spline *R*-matrix, 17CC	Present
	42.864	0.225	*B*-spline *R*-matrix, 31CC	Present
$2p3d4p\ ^4S$	44.002	8.06	*B*-spline complex rotation	Brandefelt and Lindroth (2002)
	44.017	3.31	*B*-spline *R*-matrix, 17CC	Present
	44.011	3.99	*B*-spline *R*-matrix, 31CC	Present
$2p3s3p\ ^4D$	42.985	34.3	Complex scaled CI	Sanz-Vicario and Lindroth (2002)
	42.981	33.8	*B*-spline *R*-matrix, 17CC	Present
	42.980	35.0	*B*-spline *R*-matrix, 31CC	Present

end of the region covered by our target states, and therefore the accuracy of the CC calculations in this region is not reliable. However, the extended 31CC calculation gives the width (see table 2) which also differs considerably from the value of Brandefelt and Lindroth (2002).

3.2. ^4P *photodetachment cross section*

The cross section to the final ^4P state is presented in figure 3. The general profile of our cross section agrees closely with the results of Zhou *et al* (2001a) and Sanz-Vicario and Lindroth (2002). First, we examine the energy region below the opening of the 1s detachment threshold. A strong Feshbach resonance is located here that dominates the spectrum. This resonance is assigned to the lowest triply excited state, $He^-\ 2s2p^2\ ^4P$, and well characterized by several methods (see table 2). Our 17CC calculation gives a position which is ∼20 meV higher than the results of the most recent calculations, and our width is ∼5% larger. Close agreement of widths for the $2s2p^2\ ^4P$ resonance obtained from different calculations can lead to the conclusion that the parameters of this triply excited state are defined quite accurately (Sanz-Vicario and Lindroth 2002). However, our extended results, with the inclusion of additional scattering channels, lead to further increasing of the widths, mainly due to the opening of additional decay channels. This indicates the slow convergence of close coupling expansions for resonance parameters that will be discussed latter.

Table 3. Energy, width and decay mode for He^- resonances obtained in the 31CC (first row) and 17CC (second row) approximations.

Resonance	E (eV)	W (meV)	Decay mode (%)					
^{4}S(1)	42.864	0.275	51.3	2s2p ^{3}P^o	13.6	1s5s ^{3}S	9.9	1s4s ^{3}S
	42.862	0.168	80.0	2s2p ^{3}P^o	13.4	1s3p ^{3}P^o		
^{4}S(2)	43.306	235	47.5	2p^2 ^{3}P	40.1	2s2p ^{3}P^o		
	43.316	244	49.6	2p^2 ^{3}P	38.5	2s2p ^{3}P^o		
^{4}S(3)	43.362	3.05	43.4	2s3p ^{3}P^o	31.3	2s2p ^{3}P^o		
	43.366	3.42	53.4	2s3p ^{3}P^o	40.7	2s2p ^{3}P^o		
^{4}S(4)	44.011	3.99	38.1	2s3s ^{3}S	29.9	2s3p ^{3}P^o	15.4	2p3p ^{3}D
	44.017	3.31	36.6	2s3s ^{3}S	29.9	2s3p ^{3}P^o	16.4	2p3p ^{3}D
^{4}S(5)	47.446	392	33.9	2p3p ^{3}S	23.5	2s3s ^{3}S	10.2	2s3p ^{3}P^o
^{4}S(6)	48.753	341	26.3	2p3p ^{3}S	24.8	2p3d ^{3}F^o	24.1	2p3d ^{3}P^o
^{4}P(1)	37.685	10.8	89.4	1s2p ^{3}P^o				
	37.692	10.2	95.0	1s2p ^{3}P^o				
^{4}P(2)	43.120	27.7	61.2	2s2p ^{3}P^o	32.0	2p^2 ^{3}P		
	43.121	27.8	59.0	2s2p ^{3}P^o	33.4	2p^2 ^{3}P		
^{4}P(3)	43.333	14.0	41.2	2s2p ^{3}P^o	46.6	2p^2 ^{3}P		
	43.336	13.6	38.5	2s2p ^{3}P^o	49.4	2p^2 ^{3}P		
^{4}P(4)	43.358	2.65	50.8	2s3p ^{3}P^o	26.4	2s2p ^{3}P^o	16.2	1s5p ^{3}P^o
	43.361	3.42	53.4	2s3p ^{3}P^o	40.7	2s2p ^{3}P^o		
^{4}P(5)	48.997	141	31.1	2s3p ^{3}P^o	28.2	2s2p ^{3}P^o		
^{4}D(1)	42.980	35.0	59.7	2s3s ^{3}S	30.2	2s2p ^{3}P^o		
	42.981	33.8	61.0	2s3s ^{3}S	34.0	2s2p ^{3}P^o		
^{4}D(2)	43.353	0.0471	65.2	2s3s ^{3}S	17.3	1s5p ^{3}P^o		
	43.354	1.527	67.3	2s3s ^{3}S	25.4	2s2p ^{3}P^o		
^{4}D(3)	47.412	381	30.1	2p3d ^{3}P^o	13.9	2p3s ^{3}P^o	12.7	2p3p ^{3}P
^{4}D(4)	47.975	428	29.3	2p3p ^{3}D	12.6	2p3s ^{3}P^o	11.5	2s3p ^{3}P^o
^{4}D(5)	48.474	515	29.9	2p3p ^{3}D	18.2	2p3s ^{3}P^o	12.2	2p3p ^{3}P

The second feature in the ^{4}P cross section is the strong threshold maximum due to opening of the (2s2p ^{3}P)kp channel. All calculations give very close results in this region (which is very important in further comparison with experimental data). The same conclusion concerns the next step-wise feature in the cross section at ∼40 eV. This structure is caused by opening of the (2p^2 ^{3}P)ks and (2p^2 ^{3}P)kd channels, which describe 1s photodetachment plus 2s–2p excitation. At higher energies we observe rather strong resonance structure, presented in figure 2(b) on a larger scale. The peak dominating this part of the spectrum is a strong Feshbach resonance at 43.336 eV with width 13.6 meV. As seen in table 2, all calculations report very similar results. This resonance is strongly mixed, and we tentatively assign it as the 2p3s3p ^{4}P resonance. This resonance decays almost exclusively to the 2p^2 ^{3}P and 2s2p ^{3}P channels, see table 3.

Our cross section clearly shows two small peaks on the 'wings' of the dominant 2p3s3p resonance. The time-decay and eigenphase analysis confirm that these peaks are in fact resonances. The first resonance is located at 43.120 eV and has a rather large width of 27.8 meV. This resonance correlates with the Feshbach resonance detected at 43.115 eV in the B-spline complex rotation calculations of Sanz-Vicario and Lindroth (2002), although its strength is so small that it is almost imperceptible. The second resonance is located between the He 2s3p ^{3}P^o and 2p3p ^{3}D thresholds at 43.361 eV. This feature correlates well with the small maximum at 43.360 eV in the cross section obtained by Sanz-Vicario and Lindroth (2002). However, these authors do not identify this maximum with a resonance but rather a threshold maximum. It is interesting to note that the *R*-matrix calculation by Zhou *et al* (2001a) does not predict any of the above resonances, and Sanz-Vicario and Lindroth (2002) concluded that 'the method of complex scaling proves to be more resourceful to locate the resonances'. From our point of view, the reason is simply that the present *R*-matrix calculations and complex rotation calculations by Sanz-Vicario and Lindroth (2002) include the short-range correlation to a larger extent than the *R*-matrix calculations of Zhou *et al* (2001a). In the *R*-matrix calculations, short-range correlation comes from the target wavefunctions and the $(N + 1)$-electron terms in the CC expansion (equation (1)). So incorporation of additional correlation corrections through accurate target wavefunctions seems to be very important for accurately predicting small resonance features. The last feature in the region of the $2l3l'$ target states is observed near the 2p3p ^{3}P threshold. According to our time-delay analysis, we identify this structure as a cusp effect, whereas Zhou *et al* (2001a) suggested instead the existence of a 2s3p4s ^{4}P resonance just below the 2p3p ^{3}P threshold (the suggested assignment appears to be in error because this resonance is located far above the 2s3p threshold and should therefore be a 4s shape resonance).

3.3. ^{4}D photodetachment cross section

Figure 4 shows the photodetachment cross section to the final ^{4}D state. The first peak results from the (2s2p ^{3}P)kp channel and increases rapidly from threshold to a maximum of about 18.8 Mb. This value is slightly less than the value of 22 Mb from the *R*-matrix calculations of Zhou *et al* (2001a), but as a whole the agreement between different calculations is satisfactory. Between 43 and 44 eV, some structure in the ^{4}D cross section exists. To understand the details, the cross section in this region is presented in figure 4(b) in more detail. The dominant feature in this energy region is a huge maximum of about 20 Mb at 42.981 eV, just above the 2s3s ^{3}S threshold. The major discrepancy between difference calculations arises from the interpretation of this maximum. Zhou *et al* (2001a) reiterate that this is definitely not a resonance, but a nonresonant transition, 1s2s2p ^{4}P^o–(2s3s ^{3}S)kd ^{4}D, starting at zero from threshold because it is a photodetachment, and having its maximum several tenths of an electronvolt above threshold owing to the d-wave angular momentum barrier. According to these authors, such a treatment would also explain the fact that the main part of the ^{4}D cross section of $\sim$12 Mb is contained in the partial (2s3s ^{3}S)kd cross section. A large contribution from the (2s2p ^{3}P)kp partial wave, $\sim$8 Mb, is explained by the significant effect of interchannel coupling within the ^{4}D manifold. On the other hand, the complex rotation method of Sanz-Vicario and Lindroth (2002) predicts that this maximum indeed has its origin in a clear and isolated *S*-matrix pole, i.e. a Feshbach resonance. Our time-delay analysis fully confirms this latter conclusion, and we identify that feature as the 2p3s3p resonance, with width 33.8 meV. As seen in table 2, our width closely agrees with the value from the complex rotation calculation. This resonance decays almost exclusively to the 2s2p ^{3}P and 2s3s ^{3}S channels (see table 3), and relative decay probabilities agree well with the channel cross sections presented by Zhou *et al* (2001a). However, the fact that this resonance is placed just above the 2s3s ^{3}S threshold leads the authors to the wrong conclusion that it is a threshold maximum.

3.4. Total cross sections and comparison with experiment

Recently, a high-resolution K-shell photodetachment measurement of the 1s2s2p ^{4}P^o state of He^- giving rise to He^+ was performed (Berrah *et al* 2002) in the photon energy range 38–44 eV using a merged synchrotron VUV photon–ion beam technique. In order to compare these experimental results to theory, it is necessary to extract the He^+-production cross sections

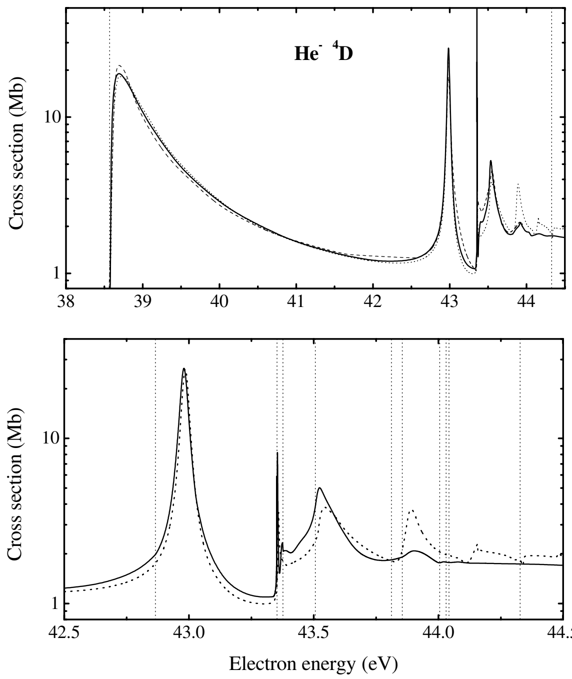

Figure 4. Calculated photodetachment cross sections to the He^- ^4D final states. Notation is the same as in figure 1.

from the total calculated photodetachment cross section. This can be done by subtracting from the total photodetachment those channels that do not result in He^+ production. These are the 1s*nl* channels, and also the $2p^2$ ^3P channel, which is metastable against autoionization and therefore decays primarily by radiation to the bound states of neutral He. The other channels are autoionizing states of He that decay almost exclusively via autoionization to He^+ (or radiatively cascade to other autoionizing states, for example, the 2p3p ^3P state). In figure 5, we compare our photodetachment cross section giving rise to He^+ with the experimental data. For the sake of comparison, we have shifted the experimental data by −140 meV to be aligned with our 2s2p $^3P^o$ threshold (the same shift has been done also by Sanz-Vicario and Lindroth (2002), indicating that the experimental energy scale may not have been calibrated precisely). The experimental results were normalized to the calculation of Zhou *et al* (2001a) at 42 eV.

The experimental data show a peak of about 15 Mb at 38.8 eV, just above the first 1s detachment threshold (He 2s2p $^3P^o$). As seen from figure 5(a), this first threshold maximum shows the poorest agreement between experimental and theoretical cross sections—theory is about a factor of two larger than experiment here. Although our first maximum is slightly less than that of Zhou *et al* (2001a), there is still large disagreement with experiment. The cross section in the first maximum is defined almost exclusively by the He^- (2s2p $^3P^o$)kp channel. It was suggested by Sanz-Vicario and Lindroth (2002) that this channel does not really participate in the production of He^+, and it is quenched by other mechanisms yet unknown. The only important approximation in the calculations is the omission of the higher members of the set of singly excited and doubly excited final states of the neutral atom, along with the continua associated with each of them. As will be shown in the next section, additional inclusion of target states (the singly excited 1s4l, 1s5l states as well as the doubly excited $3l3l'$ states)

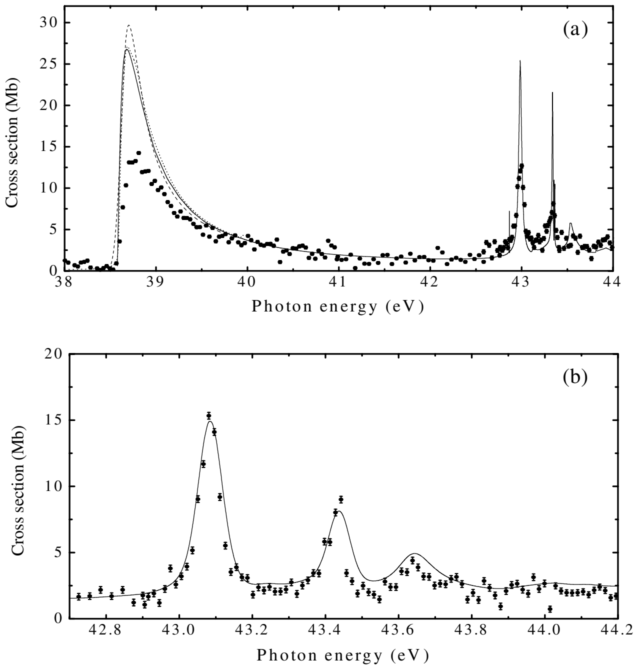

Figure 5. Total photodetachment cross section to He$^-$ from the metastable 1s2s2p ^{4}P^o state. (a) Solid curve—present R-matrix calculations, circles—experimental points from Berrah *et al* (2002). In the region of the first threshold peak comparison is given with R-matrix calculation of Zhou *et al* (2001a), dashed curve, and complex rotation CI calculation of Sanz-Vicario and Lindroth (2002), dotted curve. (b) Comparison with high resolution experimental data in the high energy region; solid curve—present photodetachment cross sections convoluted with a 70 meV FWHM Gaussian.

does not change considerably the background photodetachment cross sections, including their values in the first maximum. Inclusion of the continuum target states 2skl and 2pkl is difficult to perform in the framework of the R-matrix method. However, the complex rotation method of Sanz-Vicario and Lindroth (2002) includes such states to some extent, though it is difficult to define the correspondence between the CC expansions used in the R-matrix method and the CI expansion used in the complex rotation method. As seen in figures 1–4, the complex rotation cross sections are very close to our results for the first maximum. We can conclude that the disagreement with experiment is not caused by the truncation of the CC expansion. A similar discrepancy was observed for Li$^-$ (Kjeldsen *et al* 2001, Berrah *et al* 2001), and it remains an unsolved problem. However, it should be noted that the Li$^-$ photodetachment initial and final states have fully different configurational structure from the He$^-$ case, so the reason for the discrepancy in this case may be different.

At higher energies, experimental data show a few prominent resonances with positions that correlate well with the calculated resonance structure. A more detailed comparison with high resolution experimental data from 42.7 to 44.2 eV is presented in figure 5(b). Experimental resolution appears to lower and broaden the resonance features relative to theory. In order to perform the quantitative comparison with experiment, we convoluted the calculated cross section with a full-width at half-maximum (FWHM) Gaussian width corresponding to experimental resolution (70 meV). We now see excellent agreement between theory and experiment, both in position and magnitude of the resonance features. According to our analysis, both dominant maxima at 43.08 and 43.44 eV are due to resonances. The first peak is due to the 2p3s3p ^{4}D resonance, and the second is due to the 2p3s3p ^{4}P resonance. Our analysis contradicts the conclusion of Berrah *et al* (2002) that the first maximum is the threshold maximum.

3.5. Convergence of the close coupling expansion

The most important approximation in the CC calculations is the omission of higher target states, specifically, in the present case, the singly excited and doubly excited states of neutral He. One might expect that this omission mainly affects the higher energy photodetachment cross sections. However, due to polarization effects, omission of higher members could sometimes lead to a reduction of cross sections at small energies. In order to examine the convergence of the CC expansion in the present case, we have carried out additional calculations with both singly excited (1s4l, 1s5l) and doubly excited (3l3l') states of neutral He. The resulting CC expansion contains the 31 target states (31CC approximation). Comparison of the partial photodetachment cross sections obtained in the 17- and 31-state approximations is shown in figure 6. We see very close agreement between these cross sections, especially the background cross sections, including the magnitude and threshold maxima. We conclude that the difference between theoretical and experiment data in the first threshold peak is not caused by truncation of the CC expansion.

Increasing the number of target states leads to considerable changes in the resonance parameters. Table 3 compares the energies, widths and decay modes obtained from the two approximations. For each resonance, the first line presents results of the 31CC approximation, and the second line those from the 17CC approximation. It is difficult to give assignments for resonances based only on the R-matrix calculations, so we simply number resonances according to their energies. An increase in the number of target states leads to the appearance of new resonances, as well to changes in their parameters. The parameters of wide and strong resonances, ^{4}P(1–3) and ^{4}D(1), are relatively stable, whereas the narrow resonances, ^{4}S(1) and ^{4}P(4), are very sensitive to the approximation. In general, we may conclude a rather slow convergence of the CC expansion concerning the resonance parameters.

As expected, the 31CC calculations also reveal noticeable resonance structure in the region of the 3l3l' target states. Two broad resonances were detected in the ^{4}S partial wave. For the ^{4}P partial wave we detected only one wide resonance, 3s3p^2 ^{4}P(5), with energy and width in close agreement with those predicted by Chung (2001) using the saddle-point complex rotation method. For the ^{4}D partial wave, we detected two very broad resonances below the 3s3p ^{3}P^o excitation threshold, whereas the peak above this target state is the threshold maximum.

4. Summary

We have presented theoretical cross section results for photodetachment of He$^-$ in the region of the 1s excitation threshold. The calculations have been performed with a new extended version of the R-matrix method (Zatsarinny and Froese Fischer 2000) where a B-spline basis is employed for the representation of the continuum functions. Another distinguishing feature of the present R-matrix calculation is the use of non-orthogonal orbitals both for the construction of target wavefunctions and for the representation of scattering functions. The present calculations were undertaken in order to sort out the large discrepancies between results of previous calculations by Xi and Froese Fischer (1999) and Zhou *et al* (2001a). All calculations have been performed with different methods, but include, in principle, the same level of correlation corrections. Our calculations confirm the theoretical results of Zhou *et al*

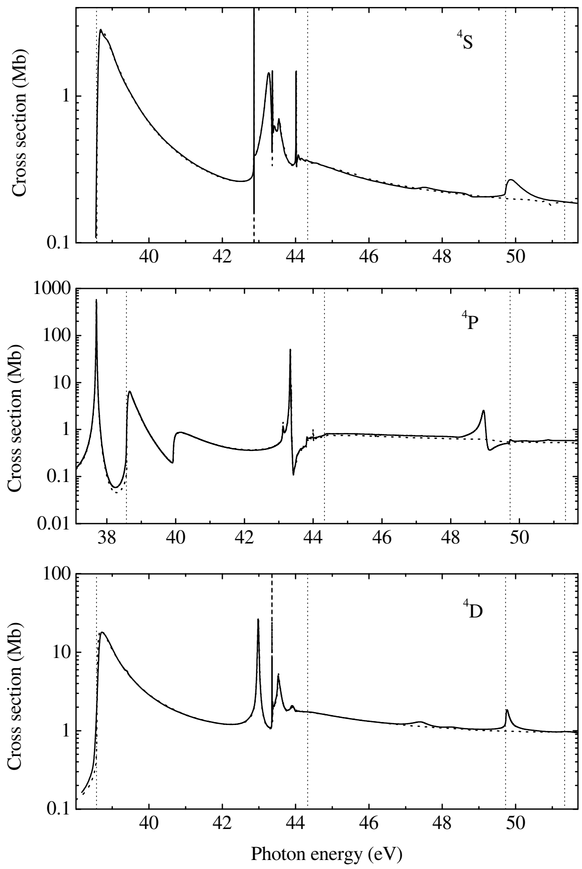

Figure 6. Comparison of the partial photodetachment cross sections obtained in the 17CC (dotted curve) and 31CC (solid curve) approximations for the ^{4}S, ^{4}P and ^{4}D final states.

(2001a). At the same time, the method used by Xi and Froese Fischer (1999), direct solution of the CC equations in the B-spline basis, gives excellent results in the low energy region (Xi and Froese Fischer 1996).

We obtained good agreement with the experimental cross section of Berrah *et al* (2002), especially in the higher energy region, where the observed resonance structure is fully interpreted from the present calculations. The remaining discrepancy is in the region of the first threshold maximum, where the theoretical cross section exceeds the experimental value by a factor of two. In order to resolve this discrepancy, we carried out CC calculations with additional target states. However, the inclusion of additional bound, as well as autoionizing, target states does not lead to significant changes in the cross sections near the first threshold maximum. This may be due to our omission of the $2lkl$ continuum target states. However, the complex scaling method used by Sanz-Vicario and Lindroth (2002) includes such target states, but still gives a very close result to ours for the threshold maximum. Additional experimental and theoretical studies are needed to resolve this existing discrepancy.

In contrast to the background cross section, the resonance structure was found to be much more sensitive to the approximation used. It is interesting to note that many resonance features were given fully different classifications in the different calculations. We believe that the present calculations are more sophisticated in this respect and adequately reproduce the observed resonance structure. In all, we detected and found energies and widths for 15 triply excited states in He^- in the region of the $2l3l'$ and $3l3l'$ excitation thresholds.

Acknowledgment

This research was supported by the US Department of Energy.

References

Amusia M Ya, Gribakin G F, Ivanov V K and Chernishova L V 1990 *J. Phys. B: At. Mol. Opt. Phys.* **23** 385
Bachau H, Cormier E, Decleva P, Hansen J E and Martin F 2001 *Rep. Prog. Phys.* **64** 1815
Berrah N *et al* 2001 *Phys. Rev. Lett.* **87** 253002
Berrah N, Bozek J D, Turri G, Akerman G, Rude B, Zhou H L and Manson S T 2002 *Phys. Rev. Lett.* **88** 93 001
Berrington K A, Eissner W B and Norrington P N 1995 *Comput. Phys. Commun.* **41** 75
Brandefelt N and Lindroth E 2002 *Phys. Rev.* A **65** 32 503
Buckman S J and Clark C W 1994 *Rev. Mod. Phys.* **66** 539
Burke P G and Berrington K A (ed) 1993 *Atomic and Molecular Processes: an R-Matrix Approach* (Bristol: Institute of Physics Publishing)
Bylicki M and Nicolaides C A 1995 *Phys. Rev.* A **51** 204
Bylicki M and Pestka G 1996 *J. Phys. B: At. Mol. Opt. Phys.* **29** L353
Chen M-K 1994 *J. Phys. B: At. Mol. Opt. Phys.* **27** 4847
Chung K T 1995 *Phys. Rev.* A **51** 844
Chung K T 2001 *Phys. Rev.* A **64** 52 503
Covington A M *et al* 2001 *J. Phys. B: At. Mol. Opt. Phys.* **34** L735
Crees M A 1980 *Comput. Phys. Commun.* **19** 103
Ho Y K 1993 *Phys. Rev.* A **48** 3598
Ivanov V K 1999 *J. Phys. B: At. Mol. Opt. Phys.* **32** R67
Ivanov V K, Krukovskaya L P and Kashenock G Yu 1998 *J. Phys. B: At. Mol. Opt. Phys.* **31** 239
Kim D-S, Zhou H-L and Manson S T 1997 *J. Phys. B: At. Mol. Opt. Phys.* **30** L1
Kjeldsen H, Andersen P, Folkmann F and Andersen T 2001 *J. Phys. B: At. Mol. Opt. Phys.* **34** L353
Kono A and Hattori S 1984 *Phys. Rev.* A **29** 2981
Kristensen P, Pedersen U V, Petrunin V V, Andersen T and Chung K T 1997 *Phys. Rev.* A **55** 978
Lindroth E 1994 *Phys. Rev.* A **49** 4473
Sanz-Vicario J L and Lindroth E 2002 *Phys. Rev.* A **65** 060703
Smith F T 1960 *Phys. Rev.* **118** 349
Xi J and Froese Fischer C 1996 *Phys. Rev.* A **53** 3169
Xi J and Froese Fischer C 1999 *Phys. Rev.* A **59** 307
Zatsarinny O 1996 *Comput. Phys. Commun.* **98** 235
Zatsarinny O and Froese Fischer C 1999 *Comput. Phys. Commun.* **124** 247
Zatsarinny O and Froese Fischer C 2000 *J. Phys. B: At. Mol. Opt. Phys.* **33** 313
Zatsarinny O and Tayal S S 2001a *J. Phys. B: At. Mol. Opt. Phys.* **34** 1299
Zatsarinny O and Tayal S S 2001b *J. Phys. B: At. Mol. Opt. Phys.* **34** 3383
Zhou H L, Manson S T, Vo Ky L, Hibbert A and Feautrier N 2001a *Phys. Rev.* A **64** 12 714
Zhou H L, Manson S T, Vo Ky L, Feautrier N and Hibbert A 2001b *Phys. Rev. Lett.* **87** 23 001